Item 830-H-15

NAS 1.60:1269

NASA Technical Paper 1269

COMPLETED

ORIGINAL

Buckling and Structural Efficiency of Sandwich-Blade Stiffened Composite Compression Panels

Manuel Stein and Jerry G. Williams

SEPTEMBER 1978

NASA

40

Item 83C-H-15

NASA Technical Paper 1269

Buckling and Structural Efficiency of Sandwich-Blade Stiffened Composite Compression Panels

Manuel Stein and Jerry G. Williams
Langley Research Center
Hampton, Virginia

National Aeronautics
and Space Administration

**Scientific and Technical
Information Office**

1978

SUMMARY

The minimum-mass structural efficiency curve is determined for sandwich-blade stiffened composite compression panels subjected to buckling and strength constraints. High structural efficiencies are attainable for this type of construction. A method of analysis is presented for the buckling of panels of this configuration which shows that buckling of such panels is strongly dependent on the through-the-thickness transverse shearing of the stiffener. Experimental results are presented from seven test specimens made of layered graphite/epoxy having stiffeners of sandwich construction with an aluminum honeycomb core, and there is good agreement between theory and experiment.

INTRODUCTION

Determination of the minimum mass of a stiffened structural panel constructed of laminated filamentary materials to carry a specific compression load in the plane of the panel is an important design problem in aerospace applications. Stiffened panels having open-section stiffeners are generally easier to inspect and fabricate than panels having closed-section stiffeners. Conventional open-section stiffened panels are not as efficient, however, as closed-section stiffened panels (ref. 1). One way to increase the performance of open-section stiffened panels is by using sandwich-blade stiffeners. In this configuration the webs of blade stiffeners are composed of faces of high-strength material bonded to a low-density core such as aluminum honeycomb. By moving the high-strength material out from the blade midsurface the critical twisting and local buckling strains can be increased without appreciably increasing the total structural mass. Some of the advantage resulting from moving the high-strength material out from the midsurface is offset by the decrease in stiffness due to one face shearing with respect to the other. This through-the-thickness transverse shearing depends on the shear stiffness of the core.

Simple, closed-form column and local buckling formulas which treat various buckling modes independently are adequate for the design of closed-section configurations, such as the hat-stiffener configuration (ref. 2). More sophisticated buckling analyses are required, however, to predict the buckling behavior of open-section configurations due to their more complicated stiffener twisting and rolling behavior (ref. 1). For a conventional stiffened panel acting as a column, inplane shearing stiffness of the webs of the stiffeners determines the overall transverse shearing stiffness of the column. For a stiffened panel with sandwich webs through-the-thickness shearing stiffness of the webs as well as inplane shearing stiffness of the webs must be considered. In this regard finite-element analyses are available which include all the effects needed. Such analyses, however, typically have execution times that are longer than desirable for the many calculations required in a structural efficiency study. Accordingly, to fill this need, a simplified, efficient, and reasonably accurate analysis has been derived and is presented in this paper for buckling of laminated sandwich-blade stiffened panels.

In addition, the paper contains a design procedure based on the newly derived analysis which is used to determine the minimum mass necessary to carry a prescribed ratio of compressive load to panel length for graphite/epoxy sandwich-blade panels, and results are presented as structural efficiency plots and are compared with previous results. The design variables are the panel dimensions and ply thicknesses, and the constraints are buckling and material allowable strength. The validity of the analytical derivations is established by comparison with a finite-element structural analysis and with test results for seven typical panels.

SYMBOLS

A	panel plan area
A_i	cross-sectional area of ith segment
$A_{11}, A_{12}, A_{22}, A_{66}$	inplane plate stiffnesses, see equations (A3)
A_{44}, A_{55}	transverse shearing stiffnesses, see equations (A6)
b	panel width
b_i	width of panel segment i
$D_{11}, D_{12}, D_{22}, D_{66}$	bending stiffnesses, see equations (A3)
E	Young's modulus
G	shear modulus
h	mesh spacing
I_1, I_2, I_p	moments of inertia in loaded and unloaded directions and polar moment of inertia of beam element
J	torsion constant
L	panel length
M_x, M_y, M_{xy}	moments per unit length
m	number of buckles along length
N	axial stress resultant of panel
N_x, N_y, N_{xy}	stress resultants

n	integer
Q_x, Q_y	transverse shear stress resultants
t_i	thickness of layer i
u,v,w	displacements in x,y,z directions, respectively
W	panel mass
x	axial coordinate
y_i	cross-sectional coordinate along segment i
β_x, β_y	rotations of normal in web
Γ	warping constant
γ_{xz}, γ_{yz}	transverse shearing strains
Δ_{ij}	Kroneker delta, 1 if $i = j$ or 0 if $i \neq j$
ϵ	axial strain at buckling
$\epsilon_x, \epsilon_y, \gamma_{xy}$	strains
θ	angle of twist
$\kappa_x, \kappa_y, \kappa_{xy}$	curvatures

MINIMUM-MASS PANEL DESIGN

Design Procedure

A computational procedure was developed for the design of minimum-mass sandwich-blade stiffened panels loaded in axial compression. Nonlinear mathematical programing techniques reported in reference 3 are used in this design procedure in which the cross-sectional dimensions of the panel are the design variables and buckling and material strength are the constraints. The buckling analysis is provided by the present theory and the strength analysis by maximum allowable strain. In design studies the panel length is fixed at 76.2 cm. In the present analysis it is assumed that the compression panel is simply supported and has many stiffeners spaced along its width, so that the structural behavior can be modeled by a typical repeating element. The geometry and design variables used to represent the repeating element for the sandwich-blade configuration are shown in figure 1. The cross section is composed of four characteristic elements: (1) the skin between two adjacent attached flanges, (2) the skin and attached flange element, (3) the sandwich web, and (4) the high-stiffness cap. The sandwich web and cap constitute the stiffener. Seven

thicknesses and four width dimensions constitute the design variables for the sandwich-blade configuration with lamina ply orientation angles of 0°, 90°, and $\pm 45^{\circ}$ permitted. Orthotropic stiffnesses are assumed for all elements, and the additional coupling effects introduced by nonsymmetric layup patterns are ignored.

Design Results

The design procedure was used to determine minimum-mass designs required to carry a specified load for the sandwich-blade stiffened configurations constructed of graphite/epoxy and aluminum-honeycomb material. Material properties used in these studies are presented in table I. Thicknesses were assumed to be continuous variables (that is, an integer number of plies was not required), and neither thickness nor cross-sectional dimension design variables were constrained to minimum limits. To satisfy the strength requirement a maximum allowable axial strain (in direction of load) of 0.008 was specified.

The structural efficiency curve shown in figure 2 was developed by first generating with the design procedure seven minimum-weight designs in the load index (N/L) range from 0.3 MPa to 7 MPa. Arbitrary honeycomb-core densities ranging from 24 kg/m^3 to 160 kg/m^3 were permitted in determining the minimum mass of a panel required to carry a specified compression load. Transverse shear modulus properties for the aluminum honeycomb were taken from reference 4 and are listed in table I(b). It was found that for minimum mass the core density varied from 24 kg/m^3 for lightly loaded (N/L = 2.5 MPa) to 160 kg/m^3 for heavily loaded (N/L = 7 MPa) panels.

The structural efficiency curve for the solid graphite/epoxy blade configuration presented in figure 2 is from reference 1 in which transverse shear effects were not included. The results presented in figure 2 for the hat-stiffened configuration are taken from reference 5 and represent slightly higher material stiffness properties than were used in the present study.

Comparisons of the results shown in figure 2 show the graphite/epoxy sandwich-blade configuration to be approximately 30 percent more efficient than the graphite/epoxy solid-blade configuration (that is, the sandwich-blade configuration requires 30 percent less mass than the solid-blade configuration to carry the same load) and 15 percent less efficient than the graphite/epoxy hat-stiffened configuration. Comparing the graphite/epoxy sandwich-blade configuration results with results presented in reference 6 for aluminum-blade and hat-stiffened panels shows that the graphite/epoxy sandwich-blade configuration provides a 60-percent mass savings over the aluminum-blade design and a 50-percent mass savings over the aluminum-hat design.

A separate investigation was carried out to check the effect on the structural efficiency of blade web transverse shearing for the solid graphite/epoxy blade configuration studied in reference 1. By assuming the transverse shear modulus only one-fourth of the shear modulus (see table I) and by assigning 0° oriented graphite/epoxy material properties for the core, an efficiency curve was obtained using the present approach. The present results obtained for the graphite/epoxy solid-blade configuration are only about 3 percent heavier than

results reported in reference 1 in which through-the-thickness transverse shear effects were not included.

BUCKLING ANALYSES

Description

Accurate finite-element analyses typically have execution times that are longer than is desirable for the many calculations required in a structural efficiency study. Consequently, a rapid simplified buckling analysis at least an order of magnitude faster than available finite-element procedures has been developed. This analysis, capable of addressing the complex twisting and rolling modes of buckling behavior of sandwich-blade stiffened panels, is presented in appendix A. The analysis predicts panel buckling loads, considering a variety of buckling modes that include column buckling, stiffener twisting and rolling, and local buckling, as well as the interaction between these modes. A second analysis is presented in appendix B and applies only to local skin buckling where the blade stiffener does not deform. The analysis in appendix B is a more accurate representation for local skin buckling than that given in appendix A.

Buckling analyses developed in the appendixes consider the problem of simply supported sandwich-blade stiffened wide panels loaded in axial compression. It is assumed in the development of these analyses that the buckling of a wide multistiffened panel may be analyzed by studying the buckling response of a single repeating element of the panel cross section. The repeating element is similar to that shown in figure 1 except that the skin and attached flange have a common center line as indicated by the sketch in appendix A. For the general study in appendix A the displacement functions assumed restrict the deformations to a mode antisymmetric about the blade stiffener. For the local buckling mode study in appendix B, however, the deformations may be symmetric. Results using the theory of appendixes A and B are compared later in this paper with other theory and with experiment.

In the present analysis all through-the-thickness transverse shearing in the web in the unloaded direction is completely constrained but transverse shearing in the loaded direction is allowed. A separate analytical study not presented here showed that the buckling load of the panels investigated was not significantly affected by the assumption that the transverse shear stiffness in the unloaded direction is infinite.

Analytical Comparisons

To determine whether or not the present results are sufficiently accurate for the important modes of buckling and for various levels of transverse shearing the present computed approximate results are compared to other computed results for two typical panels. These computations are also used to indicate the significance of the transverse shearing effects. In a later section of this paper these computed results are compared with experimental results.

Typical designs for comparative study.- Two designs, which are designated as moderately and lightly loaded, are considered which are near minimum-mass proportions necessary to satisfy buckling and strength constraints for a 76.2-cm-long simply supported panel. The cross-sectional dimensions and laminate descriptions of the panel designs considered are shown in figure 3. (For bracketed expressions defining laminate layups in fig. 3, see ref. 7. HC refers to aluminum honeycomb.) The panels are of laminated graphite/epoxy construction except for the web of the blade stiffener. The web is of sandwich construction with an aluminum honeycomb core faced with plies of ±45 graphite/epoxy. The high-axial-stiffness graphite/epoxy region at the outstanding cap of the blade stiffener (away from the skin) is assumed to act as a beam attached to the blade web. Although the panel configuration shown in figure 3 has eccentricities in the skin to permit a smooth outer surface, these eccentricities of the attached flange are ignored in the analysis. The panel designated as moderately loaded is designed to carry 1.36 MN/m when the web is constructed with a honeycomb core of density 160 kg/m^3 and to carry 1.15 MN/m when constructed with a 48 kg/m^3 core density. The lightly loaded panel is designed to carry 0.53 MN/m when constructed with a 48 kg/m^3 honeycomb-core density. The buckling strains, which are based on the derivations given in appendixes A and B for the two different designs, and from which comparisons are made between the different modes of buckling, are presented in figures 4 and 5 as a function of buckle length, L/m.

Results for moderately and lightly loaded designs.- Results for the moderately loaded design plotted in figure 4 show, for the interim region of buckle length (from 7 cm to 70 cm), that the buckling strain is strongly dependent on core density and, therefore, strongly dependent on the through-the-thickness transverse shear stiffness of the stiffener: for example, for a 30-cm-long buckle length the 48 kg/m^3 density core reduces the buckling strain by 40 percent from the solution for the infinite transverse shear stiffness case. Similarly, for the same buckle length a panel with a 160 kg/m^3 core reduces the buckling strain by 18 percent. In this interim range buckling deformations involve twisting and rolling of the stiffener. In the range beyond 70 cm the buckling strain is not as strongly dependent on core density. In the range of longer buckle lengths, column effects couple with some twisting of the stiffener; then, with still longer lengths column buckling couples with conventional column transverse shearing (shearing through the depth of the stiffener but not through the stiffener thickness). In the range below 7 cm the buckling mode is local with only the skin and the attached flange deforming, and the present results are calculated using the analysis of appendix B. Of course, with the stiffener not deforming there is no effect of core density of the stiffener in this range.

Results for the lightly loaded design plotted in figure 5 have ranges similar to those indicated for the moderately loaded design. Again for the interim region of buckle length (from 7 cm to 70 cm) the buckling strain is strongly dependent on core density and, therefore, on through-the-thickness transverse shearing of the stiffener: for example, for a 30-cm-long panel the 48 kg/m^3 density core reduces the buckling strain by approximately 25 percent from the solution for the infinite transverse shear stiffness case.

In each of the design studies the honeycomb core was oriented with the stiffer direction parallel to the load axis of the panel (that is, along the

length of the panel; see table I). Reversing this orientation was found to decrease the calculated buckling strain in the interim stiffener-twisting-mode/stiffener-rolling-mode range by approximately 15 percent. To achieve maximum load, therefore, it is recommended that the core be oriented so that its stiffest direction is along the load axis.

Comparisons with BUCLASP2.- When the honeycomb core is very dense, transverse shearing is suppressed and the blade stiffener web may be treated as a conventional plate. An exact-plate-analysis BUCLASP2 is available in reference 8 for the buckling of an assembly of conventional plates and beams which includes inplane shearing but does not allow through-the-thickness transverse shearing deformations. Comparison of present results and the exact results using the method of reference 8 (figs. 4 and 5) shows that the present results for infinite core density follow the same trends as exact results and agree to within a few percent throughout most of the buckle length range. In the range below 7 cm when local buckling occurs there is better agreement for moderately loaded panels (fig. 4) than for lightly loaded panels (fig. 5) because the inplane deformation of the stiffener that occurs when the faces are very thin is not modeled by the present local buckling analysis.

Comparisons with NASTRAN[1].- In order to assess the accuracy of the present analysis to account for through-the-thickness transverse shear effects comparisons have been made using the finite-element analysis code NASTRAN (ref. 9). Use of standard QUAD1 elements in NASTRAN allowed for orthotropic plate properties and isotropic transverse shearing. Comparison of results in figure 4 shows that the methods of references 8 and 9 agree for infinite core density. For finite core density there is also very good agreement between present results and the results obtained using NASTRAN.

EXPERIMENTAL RESULTS

Specimen Description and Test Technique

The moderately and lightly loaded sandwich-blade stiffened compression panel designs studied analytically in the previous section were also studied experimentally. A summary of design load and mass of the panels is given in table II, and the cross-sectional dimensions and laminate descriptions for these two designs are presented in figure 3. The specimens were tested in a two-stiffener-wide configuration as shown in figure 3 with side edges unsupported during the test. The specimen ends were potted in epoxy approximately 2.5 cm thick, were ground flat and parallel, and were tested "flat ended" for a nearly clamped-end test condition. Panels were tested in lengths ranging from 17.9 cm to 76.2 cm.

Specimens were constructed using 7.6-cm-wide preimpregnated tape of graphite in epoxy resin and aluminum honeycomb. Mechanical properties for these materials are presented in table I. Moderately loaded specimens were

---

[1]NASTRAN: Registered trademark of the National Aeronautics and Space Administration.

constructed using a honeycomb density of either 48 kg/m^3 or 160 kg/m^3. Lightly loaded specimens used a 48 kg/m^3 density core. The concentration of 0° oriented plies at the stiffener cap was laid up but not cured in a separate operation and was transferred to the stiffener as a unit. Epoxy was used to fill the honeycomb core for approximately 0.38 cm at the junctures where the honeycomb meets the skin and cap. A separate adhesive layer was positioned in the web between the honeycomb and the graphite epoxy. The entire assembly was vacuum-bagged and cured in an autoclave. Adhesive and epoxy materials for the core were not accounted for in the calculations and resulted in panels that were heavier than was estimated. Representative measurements, which are presented in table II, indicated that the panels were 5 to 33 percent heavier than calculated. The lightly loaded panels had more adhesive materials for the core than the moderately loaded panels on the basis of percent of total weight. Other measurements of the panels indicated very close to nominal dimensions. Experimental buckling strains were obtained from strain reversal data, and the mode shapes were determined from displacement-gage data and moire fringe patterns (ref. 10).

Experimental-Analytical Comparison

A comparison of experimental buckling strains and mode shapes between the results obtained using NASTRAN and the present theory is presented in table III. Graphical comparisons of the buckling strain as a function of the panel length are presented in figures 6 and 7. Analytical results using the analysis developed herein are for a simply supported infinitely wide multistiffener configuration while the NASTRAN results and experimental data are for the clamped two-stiffener configurations shown in figure 1.

Moderately loaded design.- Good agreement for buckling strains was achieved between both theories and experiments as shown in figure 6 and table III. Each of the 48 kg/m^3 honeycomb core density specimens buckled in a mode involving stiffener twisting and buckling of the skin as predicted by theory. Increasing the honeycomb core density from 48 kg/m^3 to 160 kg/m^3 increased the buckling strain by approximately 40 percent and changed the mode shape from $m = 2$ to $m = 1$ as predicted by theory. The buckling deformation pattern for the skin segments of the test panels may be interpreted using the moire fringe photographs shown in figure 8. Back-to-back strain-gage data and deflection-gage data, the results of which are not presented, helped to indicate that stiffener twisting and rolling were occurring. In recording mode shapes the buckle of the skin between stiffeners at the panel ends has been ignored for long wavelength buckling since this condition is peculiar to the clamped-end test restraint (ref. 1) and the corresponding clamped-end conditions imposed on the NASTRAN solution. Good correlation for mode shape was obtained between NASTRAN and experimental results.

Lightly loaded design.- Good agreement for buckling strains was obtained between the results from the present theory and the experimental results obtained for both of the 40-cm-long lightly loaded test panels as shown in figure 7 and table III. However, both panels buckled in a local skin mode ($m = 7$) rather than in a stiffener-twisting/skin-buckling mode ($m = 2$) as predicted by the present theory. (See table III.) A moire fringe photograph of

the buckle pattern is presented below the curve in figure 7. It is not clear why the experimental mode shapes do not agree with theory for the lightly loaded design while they did agree with theory for the moderately loaded design. From a study of figure 4, however, the minimum strain for short wavelength buckling ($L/m < 7$ cm) is close to the minimum strain for interim wavelength buckling (7 cm $< L/m <$ 70 cm) for the lightly loaded panel. Thus, the determination of the mode shape is sensitive to the detailed test conditions.

The ends of the specimens were all ground flat and parallel and tested "flat-ended" so that they are essentially clamped. The present theory assumes the ends are simply supported. In the interim range of buckle length where twisting occurs, however, the results using the present theory agree well with clamped experimental and NASTRAN results (fig. 4). Because of the good agreement between clamped test results and both simple-support and clamped theory, it is concluded that detailed boundary conditions beyond requiring zero deflections are apparently not important for the buckling of sandwich-blade stiffened panels where twisting occurs and where through-the-thickness transverse shearing is important.

CONCLUDING REMARKS

A minimum-mass study is presented for sandwich-blade stiffened compression panels subject to buckling and strength constraints. This study indicates that high structural efficiencies are attainable for open-section stiffened panels. The graphite/epoxy sandwich-blade stiffened configuration is approximately 30 percent more efficient than a graphite/epoxy nonsandwich configuration, 50 percent more efficient than an aluminum-hat stiffened configuration, and 60 percent more efficient than an aluminum-blade stiffened configuration. Analysis suitable for use in automated design is presented for the buckling of sandwich-blade stiffened compression panels. The buckling strain of sandwich-blade stiffened panels depends strongly on the transverse shear stiffness of the blade web core. The results of the buckling analysis which includes transverse shear deformations agree well with finite-element results. Buckling experiments on clamped, one-bay, graphite/epoxy panels having two sandwich-blade stiffeners with aluminum honeycomb core are also presented, and the results of the buckling analysis also agree with these experiments. Consequently, the analysis and especially the inclusion in the analysis of the effects of transverse shearing of the blade web core and the assumption that the panel consists of an infinite number of repeating bays are validated. The theoretical results using simple-support boundary conditions agree with clamped theoretical and experimental results when twisting occurs and through-the-thickness transverse shearing is important.

Langley Research Center
National Aeronautics and Space Administration
Hampton, VA 23665
August 3, 1978

APPENDIX A

BUCKLING ANALYSIS OF SANDWICH-BLADE STIFFENED COMPRESSION PANELS

Buckling of wide, simply supported, sandwich-blade stiffened panels loaded in axial compression is analyzed. The analysis predicts the buckling load considering a variety of buckling modes including column buckling, stiffener twisting and rolling, local buckling, and interaction between the modes. It is assumed that the buckling of a wide multistiffened panel may be analyzed by studying the repeating element of the panel cross section, which is shown in the following sketch:

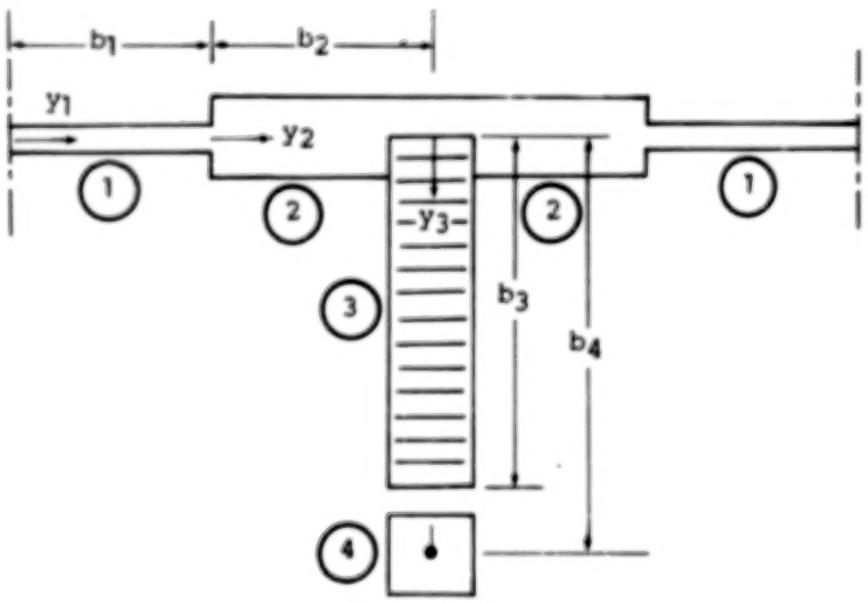

The model is composed of six basic segments: two skin (1) and two attached flange plate segments (2) located symmetrically and having a common center line, and a sandwich web plate segment (3) connected to a beam (4) forming a blade stiffener. The skin, flange, web, and beam segments are numbered 1 to 4, respectively, and the coordinate system is indicated in the sketch. The small error associated with analyzing a wide panel by studying the response of a single repeating element of the panel is discussed in reference 1.

Expressions are obtained for the buckling strain ϵ in this appendix by the method of virtual work in conjunction with assumed displacements. The virtual work of extension, bending, and the applied strain ϵ at buckling for the various plate segments may be expressed as

APPENDIX A

$$\delta\pi = \int_0^{b_i}\int_0^{L}\left[N_x\delta\varepsilon_x + N_y\delta\varepsilon_y + N_{xy}\delta\gamma_{xy} + M_x\delta\kappa_x + M_y\delta\kappa_y + M_{xy}\delta\kappa_{xy} - \varepsilon\left(A_{11} - \frac{A_{12}^2}{A_{22}}\right)(w_{,x}\delta w_{,x} + v_{,x}\delta v_{,x})\right] dx\,dy \tag{A1}$$

where the N's and M's are the stress resultants and moments; the ε's, γ_{xy}, and κ's are the strains and curvatures; and w and v are deformations that occur during buckling. The axial length of the panel is L, and the width of each segment is b_i. The strains and curvatures are given in terms of the displacements as follows:

$$\left.\begin{aligned} \varepsilon_x &= u_{,x} & \kappa_x &= -w_{,xx} \\ \varepsilon_y &= v_{,y} & \kappa_y &= -w_{,yy} \\ \gamma_{xy} &= u_{,y} + v_{,x} & \kappa_{xy} &= -2w_{,xy} \end{aligned}\right\} \tag{A2}$$

The stress-strain and moment-curvature relations are:

$$\left.\begin{aligned} N_x &= A_{11}\varepsilon_x + A_{12}\varepsilon_y & M_x &= D_{11}\kappa_x + D_{12}\kappa_y \\ N_y &= A_{22}\varepsilon_y + A_{12}\varepsilon_x & M_y &= D_{22}\kappa_y + D_{12}\kappa_x \\ N_{xy} &= A_{66}\gamma_{xy} & M_{xy} &= D_{66}\kappa_{xy} \end{aligned}\right\} \tag{A3}$$

In order to account for transverse shearing of the blade stiffener, the following work of the shearing forces must be added to the virtual work expression for the blade web segment

$$\int_0^{b_3}\int_0^{L}(Q_x\delta\gamma_{xz} + Q_y\delta\gamma_{yz})\,dx\,dy \tag{A4}$$

For the web segment the curvatures are redefined to be

$$\left.\begin{aligned} \kappa_x &= \beta_{x,x} \\ \kappa_y &= \beta_{y,y} \\ \kappa_{xy} &= \beta_{x,y} + \beta_{y,x} \end{aligned}\right\} \tag{A5}$$

APPENDIX A

The additional strain-displacement and stress-strain relations for the web are

$$\left.\begin{aligned} \gamma_{xz} &= \beta_x - w,_x & Q_x &= A_{44}\gamma_{xz} \\ \gamma_{yz} &= \beta_y - w,_y & Q_y &= A_{55}\gamma_{yz} \end{aligned}\right\} \tag{A6}$$

For the beam the virtual work is

$$\int_0^L \left[EI_1 w,_{xx}\delta w,_{xx} + EI_2 v,_{xx}\delta v,_{xx} + E\Gamma\theta,_{xx}\delta\theta,_{xx} + GJ\theta,_x\delta\theta,_x + EAu,_x\delta u,_x \right.$$

$$\left. - \epsilon EA\left(w,_x\delta w,_x + v,_x\delta v,_x + \frac{I_p}{A}\,\theta,_x\delta\theta,_x \right) \right] dx \tag{A7}$$

where EI_1 is the beam bending stiffness about the y_3 axis, EI_2 the beam bending stiffness about an axis in the cross-section perpendicular to the y_3 axis, $E\Gamma$ is the warping stiffness, GJ the torsional stiffness, EA the extensional stiffness, I_p the polar moment of inertia, and A the cross-sectional area of the beam.

The total virtual work is equal to the sum of the virtual work for each of the six segments. By substituting the expressions (A2), (A3), (A5), and (A6) for stress resultants and moments and the strains and the curvatures, the virtual work equation can be expressed in terms of the displacements u, v, and w for plate segments in the skin and in terms of u, v, w, β_x, and β_y for the web plate segment in the blade stiffener. By requiring that the beam be attached firmly to the end of the web of the blade stiffener, the u, v, w, and θ deformations of the beam are given in terms of the deformations of the web. A characteristic value problem for the lowest applied strain ϵ (the buckling strain) is obtained by considering particular expressions for the displacements that satisfy geometric boundary and continuity conditions. The displacements for each of the plate segments that have been chosen have the following form with the following arbitrary displacement coefficients U, U_3, V, W, W_3, W_{30}, X, X_3, X_{30}, and Y, plus arbitrary parameters λ and γ:

Segment — Displacements

$$1 \qquad \left.\begin{aligned} u &= U\cos\frac{m\pi x}{L} \\ v &= 0 \\ w &= -\left(V + b_2 W + \frac{2b_1}{\pi}\,W\cos\frac{\pi y_1}{2b_1} \right)\sin\frac{m\pi x}{L} \end{aligned}\right\} \tag{A8}$$

APPENDIX A

Segment 2 — Displacements

$$\left.\begin{aligned} u &= U \cos \frac{m\pi x}{L} \\ v &= 0 \\ w &= -(V + Wb_2 - Wy_2) \sin \frac{m\pi x}{L} \end{aligned}\right\} \tag{A9}$$

Segment 3 — Displacements

$$\left.\begin{aligned} u &= (U + U_3 y_3) \cos \frac{m\pi x}{L} \\ v &= V \sin \frac{m\pi x}{L} \\ w &= \left[W_3 \sin \frac{\lambda y_3}{b_3} + W_{30} \left(1 - \cos \frac{\gamma y_3}{b_3} \right) \right] \sin \frac{m\pi x}{L} \\ \beta_x &= \left(X + X_3 \sin \frac{\lambda y_3}{b_3} + X_{30} \cos \frac{\gamma y_3}{b_3} \right) \cos \frac{m\pi x}{L} \\ \beta_y &= \left(W \cos \frac{\lambda y_3}{b_3} + Y \sin \frac{\gamma y_3}{b_3} \right) \sin \frac{m\pi x}{L} \end{aligned}\right\} \tag{A10}$$

The displacements of the beam are given in terms of the displacements of segment 3 according to

$$\left.\begin{aligned} u &= u(b_3) - (b_4 - b_3) v_{,x}(b_3) \\ v &= v(b_3) \\ w &= w(b_3) + (b_4 - b_3) \beta_y(b_3) \\ \theta &= \beta_y(b_3) \end{aligned}\right\} \tag{A11}$$

These displacements are chosen so that they satisfy geometric continuity between segments, simple-support boundary conditions at $x = 0, L$, and have zero slope at $y_1 = 0$ and the corresponding point on the other side of the repeating element. Displacement functions are chosen in the y direction that give reasonable results for buckling in the local, stiffener-twisting, and column modes.

APPENDIX A

By assuming the expressions given for w in segments 1 and 2, accuracy in the local (skin-only) mode has been sacrificed for simplicity. A more accurate solution for local skin buckling is presented in appendix B.

Many of the displacements assumed for the general buckling analysis presented here are zero, constant, or linear in the y direction. The skin-deflection expression has a trigonometric function in the y direction to allow local buckling and twisting. The blade displacement expressions have two trigonometric functions in the y direction plus arbitrary parameters λ and γ to allow for rolling as well as local buckling and twisting.

Because of the way the panels are constructed, it is reasonable to expect that in segment 3

$$\beta_y - w_{,y} = 0 \tag{A12}$$

at $y_3 = 0, b_3$. As a consequence of this assumption

$$\left.\begin{aligned} W &= \frac{\lambda}{b_3} W_3 \\ Y &= \frac{\gamma}{b_3} W_{30} \end{aligned}\right\} \tag{A13}$$

and, therefore, in effect it is assumed that the transverse shearing strain γ_{yz} is zero in the web. The solution is then independent of A_{55}, and the number of unknown displacement coefficients is reduced from 10 to 8.

The stability equations that result from the method of virtual work for this problem can be identified from

$$\begin{bmatrix} a_{11} & a_{12} & a_{13} & 0 & 0 & 0 & 0 & 0 \\ & a_{22} & a_{23} & 0 & 0 & 0 & 0 & 0 \\ & & a_{33} - \varepsilon b_{33} & a_{34} - \varepsilon b_{34} & 0 & 0 & 0 & 0 \\ & & & a_{44} - \varepsilon b_{44} & a_{45} - \varepsilon b_{45} & a_{46} & a_{47} & a_{48} \\ & & & & a_{55} - \varepsilon b_{55} & a_{56} & a_{57} & a_{58} \\ & & & & & a_{66} & a_{67} & a_{68} \\ & \text{Symmetric} & & & & & a_{77} & a_{78} \\ & & & & & & & a_{88} \end{bmatrix} \begin{Bmatrix} U \\ U_3 \\ V \\ W_3 \\ W_{30} \\ X \\ X_{30} \\ X_3 \end{Bmatrix} = 0 \tag{A14}$$

APPENDIX A

wherein what follows $\bar{A} = A_{11} - \left(A_{12}^2/A_{22}\right)$ and subscripts have been added to $\bar{A}$, A_{ij}, and D_{ij} to indicate the segment represented:

$$a_{11} = \left(\frac{m\pi}{L}\right)^2 (2A_{111}b_1 + 2A_{112}b_2 + A_{113}b_3 + EA)$$

$$a_{12} = \left(\frac{m\pi}{L}\right)^2 \left(\frac{1}{2} A_{113}b_3^2 + EAb_3\right)$$

$$a_{13} = -\left(\frac{m\pi}{L}\right)^3 (b_4 - b_3)EA$$

$$a_{22} = \left(\frac{m\pi}{L}\right)^2 \left(\frac{1}{3} A_{113}b_3^3 + EAb_3^2\right) + A_{663}b_3$$

$$a_{23} = \frac{m\pi}{L} A_{663}b_3 - \left(\frac{m\pi}{L}\right)^3 (EAb_3)(b_4 - b_3)$$

$$a_{33} = 2\left(\frac{m\pi}{L}\right)^4 \left[D_{111}b_1 + D_{112}b_2 + EI_2 + EA(b_4 - b_3)^2\right] + \left(\frac{m\pi}{L}\right)^2 A_{663}b_3$$

$$b_{33} = \left(\frac{m\pi}{L}\right)^2 (\bar{A}_3b_3 + 2\bar{A}_1b_1 + 2\bar{A}_2b_2 + EA)$$

$$a_{34} = 2\frac{\lambda}{b_3}\left(\left(\frac{m\pi}{L}\right)^4 \left\{D_{111}\left[b_1b_2 + \left(\frac{2b_1}{\pi}\right)^2\right] + \frac{1}{2} D_{112}b_2^2\right\} + \left(\frac{m\pi}{L}\right)^2 D_{121}\right)$$

$$b_{34} = 2\frac{\lambda}{b_3}\left(\frac{m\pi}{L}\right)^2 \left\{\bar{A}_1\left[b_1b_2 + \left(\frac{2b_1}{\pi}\right)^2\right] + \frac{1}{2} \bar{A}_2b_2^2\right\}$$

$$a_{44} = \left(\frac{m\pi}{L}\right)^2 \left[\frac{1}{2} A_{44}b_3\left(1 - \frac{\cos\lambda \sin\lambda}{\lambda}\right) + EI_1 \sin^2\lambda\right] + \left(\frac{\lambda}{b_3}\right)^2 F_1$$

$$+ 2\frac{\lambda}{b_3}\left(\frac{m\pi}{L}\right)^4 (b_4 - b_3) \sin\lambda \cos\lambda$$

APPENDIX A

$$b_{44} = \left(\frac{m\pi}{L}\right)^2\left[\frac{1}{2}\bar{A}_3 b_3\left(1 - \frac{\cos\lambda\sin\lambda}{\lambda}\right) + EA\sin^2\lambda + 2\frac{\lambda}{b_3}EA(b_4 - b_3)\sin\lambda\cos\lambda\right] + \left(\frac{\lambda}{b_3}\right)^2 F_2$$

$$a_{45} = \left(\frac{m\pi}{L}\right)^2 A_{44}F_3 + \left(\frac{m\pi}{L}\right)^4 EI_1\sin\lambda(1 - \cos\gamma) + \frac{\lambda}{b_3}F_4 + \frac{\gamma}{b_3}F_5$$

$$b_{45} = \left(\frac{m\pi}{L}\right)^2\left[\bar{A}_3F_3 + EA\sin\lambda(1 - \cos\gamma) + \frac{\lambda}{b_3}EA(b_4 - b_3)(1 - \cos\gamma)\cos\lambda\right] + \frac{\gamma}{b_3}F_6$$

$$a_{46} = \frac{m\pi}{L}\frac{b_3}{\lambda}(1 - \cos\lambda)\left[\left(\frac{\lambda}{b_3}\right)^2 D_{123} - A_{44}\right]$$

$$a_{47} = \frac{m\pi}{L}F_7\left[\left(\frac{\lambda}{b_3}\right)^2 D_{123} - A_{44}\right] + \frac{m\pi}{L}F_8\frac{\lambda}{b_3}D_{223}$$

$$a_{48} = \frac{m\pi}{L}F_9\left[\left(\frac{\lambda}{b_3}\right)^2 D_{123} - A_{44}\right] - \frac{\lambda}{b_3}\frac{\gamma}{b_3}D_{\epsilon 63}F_{10}$$

$$a_{55} = \left(\frac{m\pi}{L}\right)^2 A_{44}F_{11} + \left(\frac{m\pi}{L}\right)^4 EI_1(1 - \cos\gamma)^2 + 2\frac{\gamma}{b_3}EI_1\left(\frac{m\pi}{L}\right)^4(b_4 - b_3)\sin\gamma(1 - \cos\gamma) + \left(\frac{\gamma}{b_3}\right)^2 F_{12}$$

$$b_{55} = \left(\frac{m\pi}{L}\right)^2\left\{\bar{A}_3F_{11} + EA(1 - \cos\gamma)^2 + 2\frac{\gamma}{b_3}EA(b_4 - b_3)\sin\gamma(1 - \cos\gamma) + \left(\frac{\gamma}{b_3}\right)^2 EA\left[(b_4 - b_3)^2 + \frac{I_p}{A}\right]\sin^2\gamma\right\}$$

APPENDIX A

$$a_{56} = -\frac{m\pi}{L}\left[A_{44}\left(b_3 - \frac{\sin\gamma}{\gamma}\right) + D_{123}\frac{\gamma}{b_3}\sin\gamma\right]$$

$$a_{57} = -\frac{m\pi}{L}A_{44}F_3 - \left(\frac{\gamma}{b_3}\right)^2\frac{m\pi}{L}D_{123}F_9 - \left(\frac{\lambda\gamma}{b_3{}^2}\right)\frac{m\pi}{L}D_{663}F_{10}$$

$$a_{58} = -\frac{m\pi}{L}A_{44}F_{13} + \frac{\gamma}{b_3}F_{14}$$

$$a_{66} = \left(\frac{m\pi}{L}\right)^2 D_{113}b_3 + A_{44}b_3$$

$$a_{67} = \left[\left(\frac{m\pi}{L}\right)^2 D_{113} + A_{44}\right]\frac{b_3}{\lambda}(1 - \cos\lambda)$$

$$a_{68} = \left[\left(\frac{m\pi}{L}\right)^2 D_{113} + A_{44}\right]\frac{b_3}{\gamma}\sin\gamma$$

$$a_{77} = \left[\left(\frac{m\pi}{L}\right)^2 D_{113} + A_{44}\right]F_7 + D_{663}\left(\frac{\lambda}{b_3}\right)^2 F_8$$

$$a_{78} = \left[\left(\frac{m\pi}{L}\right)^2 D_{113} + A_{44}\right]F_9 - D_{663}\left(\frac{\lambda\gamma}{b_3{}^2}\right)F_{10}$$

$$a_{88} = \left[\left(\frac{m\pi}{L}\right)^2 D_{113} + A_{44}\right]F_{15} + D_{663}\left(\frac{\gamma}{b_3}\right)^2 F_{16}$$

and

$$F_1 = 2\left(\frac{m\pi}{L}\right)^4 \left\{ D_{111}\left[b_1 b_2^2 + 2\left(\frac{2b_1}{\pi}\right)^2 \left(b_2 + \frac{b_1}{4} \right) \right] + D_{112} \frac{b_2^3}{3} \right\} + 4\left(\frac{m\pi}{L}\right)^2 D_{121} \left(b_2 + \frac{b_1}{2} \right)$$
$$+ \left(\frac{\pi}{2b_1}\right)^2 D_{221} b_1 + 8\left(\frac{m\pi}{L}\right)^2 \left(D_{661} \frac{b_1}{2} + D_{662} b_2 \right) + \left(\frac{m\pi}{L}\right)^2 D_{663} F_8 + \left(\frac{\lambda}{b_3}\right)^2 D_{223} F_7$$
$$+ \left[EI_1 \left(\frac{m\pi}{L}\right)^4 (b_4 - b_3)^2 + E\Gamma \left(\frac{m\pi}{L}\right)^4 + GJ \left(\frac{m\pi}{L}\right)^2 \right] \cos^2 \lambda$$

$$F_2 = 2\left(\frac{m\pi}{L}\right)^2 \left\{ \bar{A}_1 \left[b_1 b_2^2 + 2\left(\frac{2b_1}{\pi}\right)^2 \left(b_2 + \frac{b_1}{4} \right) \right] + \bar{A}_2 \frac{b_2^3}{3} \right\}$$
$$+ EA\left(\frac{m\pi}{L}\right)^2 \cos^2 \lambda \left[(b_4 - b_3)^2 + \frac{I_p}{A} \right]$$

$$F_3 = -\frac{b_3}{2}\left[\frac{1 - \cos(\lambda - \gamma)}{\lambda - \gamma} + \frac{1 - \cos(\lambda + \gamma)}{\lambda + \gamma} \right] + \frac{b_3}{\lambda}(1 - \cos \lambda)$$

$$F_4 = EA\left(\frac{m\pi}{L}\right)^2 (b_4 - b_3)(1 - \cos \gamma) \cos \lambda$$

$$F_5 = EI_1 \left(\frac{m\pi}{L}\right)^4 (b_4 - b_3) \sin \gamma \sin \lambda + \frac{\lambda}{b_3} F_{17}$$

$$F_6 = EA\left(\frac{m\pi}{L}\right)^2 (b_4 - b_3) \sin \gamma \sin \lambda + \frac{\lambda}{b_3} F_{18}$$

$$F_7 = \frac{b_3}{2}\left(1 - \frac{\cos \lambda \sin \lambda}{\lambda} \right)$$

$$F_8 = \frac{b_3}{2}\left(1 + \frac{\cos \lambda \sin \lambda}{\lambda} \right)$$

APPENDIX A

$$F_9 = \frac{b_3}{2}\left[\frac{1 - \cos(\lambda - \gamma)}{\lambda - \gamma} + \frac{1 - \cos(\lambda + \gamma)}{\lambda + \gamma}\right]$$

$$F_{10} = \frac{b_3}{2}\left[-\frac{1 - \cos(\lambda - \gamma)}{\lambda - \gamma} + \frac{1 - \cos(\lambda + \gamma)}{\lambda + \gamma}\right]$$

$$F_{11} = \frac{b_3}{2}\left(1 + \frac{\cos\gamma \sin\gamma}{\gamma}\right) + b_3 - 2\frac{b_3}{\gamma}\sin\gamma$$

$$F_{12} = \left(\frac{m\pi}{L}\right)^2 D_{663}F_{16} + \left(\frac{\gamma}{b_3}\right)^2 D_{223}F_{15}$$

$$+ \left[EI_1\left(\frac{m\pi}{L}\right)^4 (b_4 - b_3)^2 + E\Gamma\left(\frac{m\pi}{L}\right)^4 + GJ\left(\frac{m\pi}{L}\right)^2\right]\sin^2\gamma$$

$$F_{13} = -\frac{b_3}{2}\left(1 + \frac{\cos\gamma \sin\gamma}{\gamma}\right) + \frac{b_3}{\gamma}\sin\gamma$$

$$F_{14} = -\frac{m\pi}{L}\frac{\gamma}{b_3}(D_{123}F_{15} + D_{663}F_{16})$$

$$F_{15} = \frac{b_3}{2}\left(1 + \frac{\cos\gamma \sin\gamma}{\gamma}\right)$$

$$F_{16} = \frac{b_3}{2}\left(1 - \frac{\cos\gamma \sin\gamma}{\gamma}\right)$$

$$F_{17} = \left(\frac{m\pi}{L}\right)^2 D_{663}F_{10} - \frac{\lambda\gamma}{{b_3}^2} D_{223}F_9$$

$$+ \left[EI_1\left(\frac{m\pi}{L}\right)^4 (b_4 - b_3)^2 + E\Gamma\left(\frac{m\pi}{L}\right)^4 + GJ\left(\frac{m\pi}{L}\right)^2\right]\sin\gamma\cos\lambda$$

$$F_{18} = EA\left(\frac{m\pi}{L}\right)^2\left[(b_4 - b_3)^2 + \frac{I_p}{A}\right] \sin\gamma \cos\lambda$$

The stability equations (A14) are a homogeneous set. To obtain a nontrivial solution for the buckling strain the determinant of the matrix must vanish. The buckling strain is the lowest value of the applied strain ϵ that satisfies this equation for various values of λ, γ, and m. As in reference 1, suggested trial values are $\lambda = 0.1\pi$, 0.3π, 0.5π, 0.7π, and $\gamma = \lambda + 0.5\pi$.

APPENDIX B

LOCAL BUCKLING OF SANDWICH-BLADE STIFFENED COMPRESSION PANELS

An analysis is developed for the skin-only local buckling of wide, simply supported, sandwich-blade stiffened panels loaded in axial compression. The method of analysis used is the method of virtual work in conjunction with central finite differences. For this mode of buckling the blade stiffener does not deform but serves to clamp the skin at the point of attachment. A sketch of the model studied is shown here:

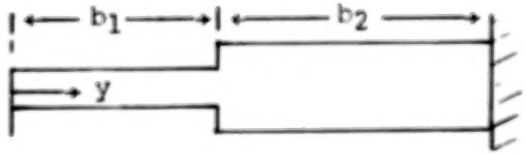

For the mode considered, the slope at $y = 0$ is zero. For this model stretching and bending are uncoupled and, for buckling, only bending must be considered. The virtual work during buckling is

$$\delta\pi = \int_0^{b_1+b_2}\int_0^{L}\left[M_x\delta\kappa_x + M_y\delta\kappa_y + M_{xy}\delta\kappa_{xy} - \epsilon\left(A_{11} - \frac{A_{12}^2}{A_{22}}\right)w_{,x}\delta w_{,x}\right]dx\,dy \qquad (B1)$$

where

$$\left.\begin{aligned} \kappa_x &= -w_{,xx} & M_x &= D_{11}\kappa_x + D_{12}\kappa_y \\ \kappa_y &= -w_{,yy} & M_y &= D_{22}\kappa_y + D_{12}\kappa_x \\ \kappa_{xy} &= -2w_{,xy} & M_{xy} &= D_{66}\kappa_{xy} \end{aligned}\right\} \qquad (B2)$$

Letting $w = W(y)\sin\dfrac{m\pi x}{L}$ in equations (B1) and (B2) and integrating over x yields

$$\delta\pi = \frac{L}{2}\int_0^{b_1+b_2}\left\{\left[D_{11}\left(\frac{m\pi}{L}\right)^4 W - D_{12}\left(\frac{m\pi}{L}\right)^2 W'' - \epsilon\bar{A}\left(\frac{m\pi}{L}\right)^2 W\right]\delta W + \left[D_{22}W'' - D_{12}\left(\frac{m\pi}{L}\right)^2 W\right]\delta W''\right.$$

$$\left. + 4\left(\frac{m\pi}{L}\right)^2 D_{66}W'\delta W'\right\}\,dy \qquad (B3)$$

where $\bar{A} = A_{11} - \left(A_{12}^2/A_{22}\right)$. In equation (B3) the derivatives are approximated using central differences as indicated in the following, and the trapezoidal rule is used for integration:

$$(W'')_n = \frac{W_{n+1} - 2W_n + W_{n-1}}{h^2} \tag{B4}$$

$$(W')_{n+\frac{1}{2}} = \frac{W_{n+1} - W_n}{h} \tag{B5}$$

where h is the uniform mesh spacing. Equation (B3) becomes

$$\delta\pi = \frac{Lh}{2}\left\{\sum_{n=0}^{N}\left[a_n\delta W_n + \frac{b_n(\delta W_{n+1} - 2\delta W_n + \delta W_{n-1})}{h^2}\right]\left(1 - \frac{\Delta_{n0} + \Delta_{nN}}{2}\right)\right.$$

$$\left. + \sum_{n=0}^{N-1} c_{n+\frac{1}{2}} \frac{\delta W_{n+1} - \delta W_n}{h}\right\} \tag{B6}$$

where, away from the boundaries:

$$\left.\begin{aligned} a_n &= \left(\frac{m\pi}{L}\right)^2\left[D_{11n}\left(\frac{m\pi}{L}\right)^2 W_n - D_{12n}\frac{W_{n+1} - 2W_n + W_{n-1}}{h^2} - c\bar{A}_n W_n\right] \\ b_n &= D_{22n}\frac{W_{n+1} - 2W_n + W_{n-1}}{h^2} - D_{12n}\left(\frac{m\pi}{L}\right)^2 W_n \\ c_{n+\frac{1}{2}} &= 4\left(\frac{m\pi}{L}\right)^2 D_{66n}\frac{W_{n+1} - W_n}{h} \end{aligned}\right\} \tag{B7}$$

and Δ_{ij} is the Kroneker delta which equals zero if the subscripts are different and one if the subscripts are the same, and D_{ij} and $\bar{A}$ have the sub-

script n that refers to nodal points. The expression (B6) for the virtual work depends on the displacements W_n specified at the nodal points within and on the boundaries from $n = 0$ to N and at the fictitious points -1 and $N+1$ outside the boundaries. To apply the method of virtual work it is necessary that the displacements W_n and the virtual displacements δW_n satisfy geometric boundary conditions. The boundary conditions specified are

Zero slope at $y = 0$ or, therefore, $W_{-1} = W_1$

Zero deflection at $y = b_1 + b_2$ or, therefore, $W_N = 0$

Zero slope at $y = b_1 + b_2$ or, therefore, $W_{N+1} = W_{N-1}$

These conditions affect the a's, b's, and c's, so that the following definitions must be used instead of the corresponding general expressions:

$$
\left.
\begin{aligned}
a_0 &= \left(\frac{m\pi}{L}\right)^2\left[D_{110}\left(\frac{m\pi}{L}\right)^2 W_0 - 2D_{120}\,\frac{W_1 - W_0}{h^2} - \epsilon\bar{A}_0 W_0\right] \\
b_0 &= 2D_{220}\,\frac{W_1 - W_0}{h^2} - D_{120}\left(\frac{m\pi}{L}\right)^2 W_0 \\
a_{N-1} &= \left(\frac{m\pi}{L}\right)^2\left[(D_{11})_{N-1}\left(\frac{m\pi}{L}\right)^2 W_{N-1} - (D_{12})_{N-1}\left(\frac{-2W_{N-1} + W_{N-2}}{h^2}\right) + \epsilon\bar{A}_{N-1}W_{N-1}\right] \\
b_{N-1} &= (D_{22})_{N-1} - \frac{2W_{N-1} + W_{N-2}}{h^2} - (D_{12})_{N-1}\left(\frac{m\pi}{L}\right)^2 W_{N-1} \\
c_{N-\frac{1}{2}} &= -4\left(\frac{m\pi}{L}\right)^2 (D_{66})_{N-\frac{1}{2}}\,\frac{W_{N-1}}{h} \\
b_N &= 2D_{22N}\,\frac{W_{N-1}}{h^2}
\end{aligned}
\right\} \qquad \text{(B8)}
$$

APPENDIX B

The virtual work becomes

$$\delta\pi = \frac{Lh}{2}\left[\left(\frac{a_0}{2} - \frac{b_1 - b_0}{h^2} - \frac{c_{1/2}}{h}\right)\delta w_0 + \left(a_1 + \frac{b_2 - 2b_1 + b_0}{h^2} - \frac{c_{3/2} - c_{1/2}}{h}\right)\delta w_1\right.$$

$$+ \ldots$$

$$\left. + \left(a_{N-1} + \frac{b_N - 2b_{N-1} + b_{N-2}}{h^2} - \frac{c_{N-\frac{1}{2}} - c_{N-\frac{3}{2}}}{h}\right)\delta w_{N-1}\right] \tag{B9}$$

Setting the virtual work equal to zero and, therefore, requiring that the coefficients of the virtual displacements vanish leads to the stability equations (for example, with $N = 8$):

$$\begin{bmatrix} a_{11} & a_{12} & a_{13} & 0 & 0 & 0 & 0 & 0 \\ & a_{22} & a_{23} & a_{24} & 0 & 0 & 0 & 0 \\ & & a_{33} & a_{34} & a_{35} & 0 & 0 & 0 \\ & & & a_{44} & a_{45} & a_{46} & 0 & 0 \\ & & & & a_{55} & a_{56} & a_{57} & 0 \\ & & & & & a_{66} & a_{67} & a_{68} \\ & \text{Symmetric} & & & & & a_{77} & a_{78} \\ & & & & & & & a_{88} \end{bmatrix} \begin{Bmatrix} w_0 \\ w_2 \\ w_3 \\ w_4 \\ w_5 \\ w_6 \\ w_7 \\ w_8 \end{Bmatrix} = 0 \tag{B10}$$

where

$$a_{11} = \frac{1}{2} D_{110}\left(\frac{m\pi}{L}\right)^4 + \left(D_{121} + D_{120} + 4D_{66\frac{1}{2}}\right)\left(\frac{m\pi}{L}\right)^2 \frac{1}{h^2} + (2D_{221} + D_{220})\frac{1}{h^4} - \frac{\epsilon}{2}\bar{A}_0\left(\frac{m\pi}{L}\right)^2$$

APPENDIX B

$$a_{22} = D_{111}\left(\frac{m\pi}{L}\right)^4 + 4\left(D_{121} + D_{66\frac{3}{2}} + D_{66\frac{1}{2}}\right)\left(\frac{m\pi}{L}\right)^2 \frac{1}{h^2}$$

$$+ (D_{222} + 4D_{221} + 2D_{220})\frac{1}{h^4} - \epsilon\bar{A}_1\left(\frac{m\pi}{L}\right)^2$$

$$a_{33} = D_{112}\left(\frac{m\pi}{L}\right)^4 + 4\left(D_{122} + D_{66\frac{5}{2}} + D_{66\frac{3}{2}}\right)\left(\frac{m\pi}{L}\right)^2 \frac{1}{h^2}$$

$$+ (D_{223} + 4D_{222} + D_{221})\frac{1}{h^4} - \epsilon\bar{A}_2\left(\frac{m\pi}{L}\right)^2$$

$$\vdots$$

$$a_{77} = D_{116}\left(\frac{m\pi}{L}\right)^4 + 4\left(D_{126} + D_{66\frac{13}{2}} + D_{66\frac{11}{2}}\right)\left(\frac{m\pi}{L}\right)^2 \frac{1}{h^2}$$

$$+ (D_{227} + 4D_{226} + D_{225})\frac{1}{h^4} - \epsilon\bar{A}_6\left(\frac{m\pi}{L}\right)^2$$

$$a_{89} = D_{117}\left(\frac{m\pi}{L}\right)^4 + \left(3D_{127} + 4D_{66\frac{15}{2}} + 4D_{66\frac{13}{2}}\right)\left(\frac{m\pi}{L}\right)^2 \frac{1}{h^2}$$

$$+ (2D_{228} + 4D_{227} + D_{226})\frac{1}{h^4} - \epsilon\bar{A}_7\left(\frac{m\pi}{L}\right)^2$$

APPENDIX B

$$a_{12} = -\left(D_{121} + D_{120} + 4D_{66\frac{1}{2}}\right)\left(\frac{m\pi}{L}\right)^2 \frac{1}{h^2} - 2(D_{221} + D_{220})\frac{1}{h^4}$$

$$\vdots$$

$$a_{78} = -\left(D_{127} + D_{126} + 4D_{66\frac{13}{2}}\right)\left(\frac{m\pi}{L}\right)^2 \frac{1}{h^2} - 2(D_{227} + D_{226})\frac{1}{h^4}$$

$$a_{13} = D_{221}\,\frac{1}{h^4}$$

$$\vdots$$

$$a_{68} = D_{226}\,\frac{1}{h^4}$$

The D's and $\bar{A}$'s must be assigned values according to the nodal point represented. In the neighborhood of the jump in stiffness all the D's and $\bar{A}$'s should be assigned values based on the segment (of width h) centered on the nodal points except for D_{66} which should be assigned a value based on the segment between nodal points.

The stability equations (B10) are a homogeneous set, and to get a nontrivial solution for the buckling strain the determinant of the matrix must vanish. The buckling strain is the lowest value of the applied strain ϵ that satisfies this equation for various values of m. Computations were based on $N = 8$.

REFERENCES

1. Williams, Jerry G.; and Stein, Manuel: Buckling Behavior and Structural Efficiency of Open-Section Stiffened Composite Compression Panels. AIAA J., vol. 14, no. 11, Nov. 1976, pp. 1618-1626.

2. Agarwal, Banarsi; and Davis, Randall C.: Minimum-Weight Designs for Hat-Stiffened Composite Panels Under Uniaxial Compression. NASA TN D-7779, 1974.

3. Jones, R. T.; and Hague, D. S.: Application of Multivariable Search Techniques to Structural Design Optimization. NASA CR-2038, 1972.

4. Design Curves for the Preliminary Selection of Honeycomb Sandwich Structures. TSB 121, Hexcel Products Inc., Jan. 1965.

5. Stroud, W. Jefferson; Agranoff, Nancy; and Anderson, Melvin S.: Minimum-Mass Design of Filamentary Composite Panels Under Combined Loads: Design Procedure Based on a Rigorous Buckling Analysis. NASA TN D-8417, 1977.

6. Williams, Jerry G.; and Mikulas, Martin M., Jr.: Analytical and Experimental Study of Structurally Efficient Composite Hat-Stiffened Panels Loaded in Axial Compression. NASA TM X-72813, 1976. (Also available as AIAA Paper No. 75-754.)

7. Advanced Composites Design Guide. Volume III - Manufacturing. Third ed., Air Force Materials Lab., U.S. Air Force, Jan. 1973. (Available from DDC as AD 916 681L.)

8. Viswanathan, A. V.; and Tamekuni, M.: Elastic Buckling Analysis for Composite Stiffened Panels and Other Structures Subjected to Biaxial Inplane Loads. NASA CR-2216, 1973.

9. The NASTRAN User's Manual (Level 16.0). NASA SP-222(03), 1976.

10. Dykes, B. C.: Analysis of Displacements in Large Plates by the Grid-Shadow Moiré Technique. Experimental Stress Analysis and Its Influence on Design, M. L. Meyer, ed., Inst. Mech. Eng., c.1971, pp. 125-134.

TABLE I.- MATERIAL PROPERTIES

(a) Graphite/epoxy

Modulus in fiber direction, GPa	131
Modulus normal to fibers, GPa	13.0
Shear modulus, GPa	6.41
Major Poisson's ratio	0.38
Density, Mg/m^3	1.52
Thickness, mm/ply	0.14

(b) Aluminum honeycomb[a]

Density, kg/m^3	Major transverse shear modulus, GPa	Minor transverse shear modulus, GPa
24	0.117	0.062
32	.159	.083
48	.262	.138
64	.393	.193
80	.524	.262
96	.641	.324
112	.786	.372
128	.938	.427
144	1.08	.469
160	1.21	.483

[a]Reference 4.

TABLE II.- DESIGN LOAD AND MASS FOR SIMPLY SUPPORTED PANELS 76.2 cm LONG

Panel	Honeycomb-core density, kg/m^3	Theoretical buckling load, MN/m	Theoretical buckling strain	Mass/Plan area, kg/m^2	
				Calculated	Measured
Moderately loaded	48	1.15	0.0044	6.93	7.31
	160	1.36	.0051	7.30	8.39
Lightly loaded	48	.53	.0046	4.29	5.73

TABLE III.- BUCKLING STRAINS AND MODES

Panel length, cm	Honeycomb-core density, kg/m^3	Strain, ε			Buckles along panel length		
		Present theory	NASTRAN	Experiment	Present theory	NASTRAN	Experiment
Moderately loaded panel design							
17.9	48	0.0047	0.0047	0.0045	1	4	3
26.7	48	.0043	.0050	.0048	1	[a]1	[a]1
30.?	48	.0043	.0052	.0042	1	[a]2	[a]1
76.2	48	.0044	.0040	.0041	2	[a]2	[a]2
76.2	160	.0051	.0051	.0058	1	[a]1	[a]1
Lightly loaded panel design							
40.6	48	0.0046		0.0052	2		7
40.6	48	.0046		.0050	2		7

[a]Ignores buckle at panel ends resulting from clamped-end biaxial stress field.

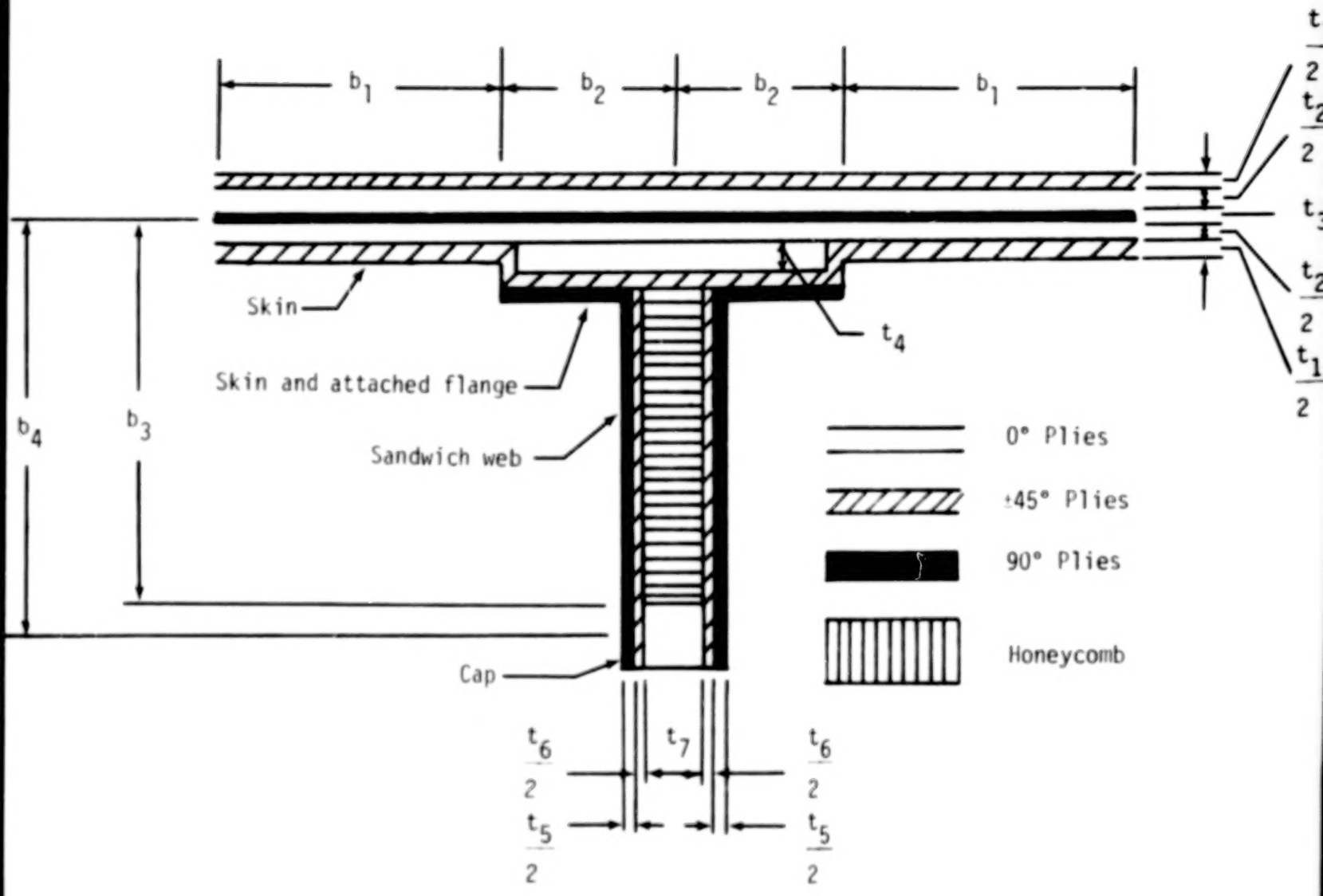

Figure 1.- Configuration options and design variables used in minimum-mass design procedure.

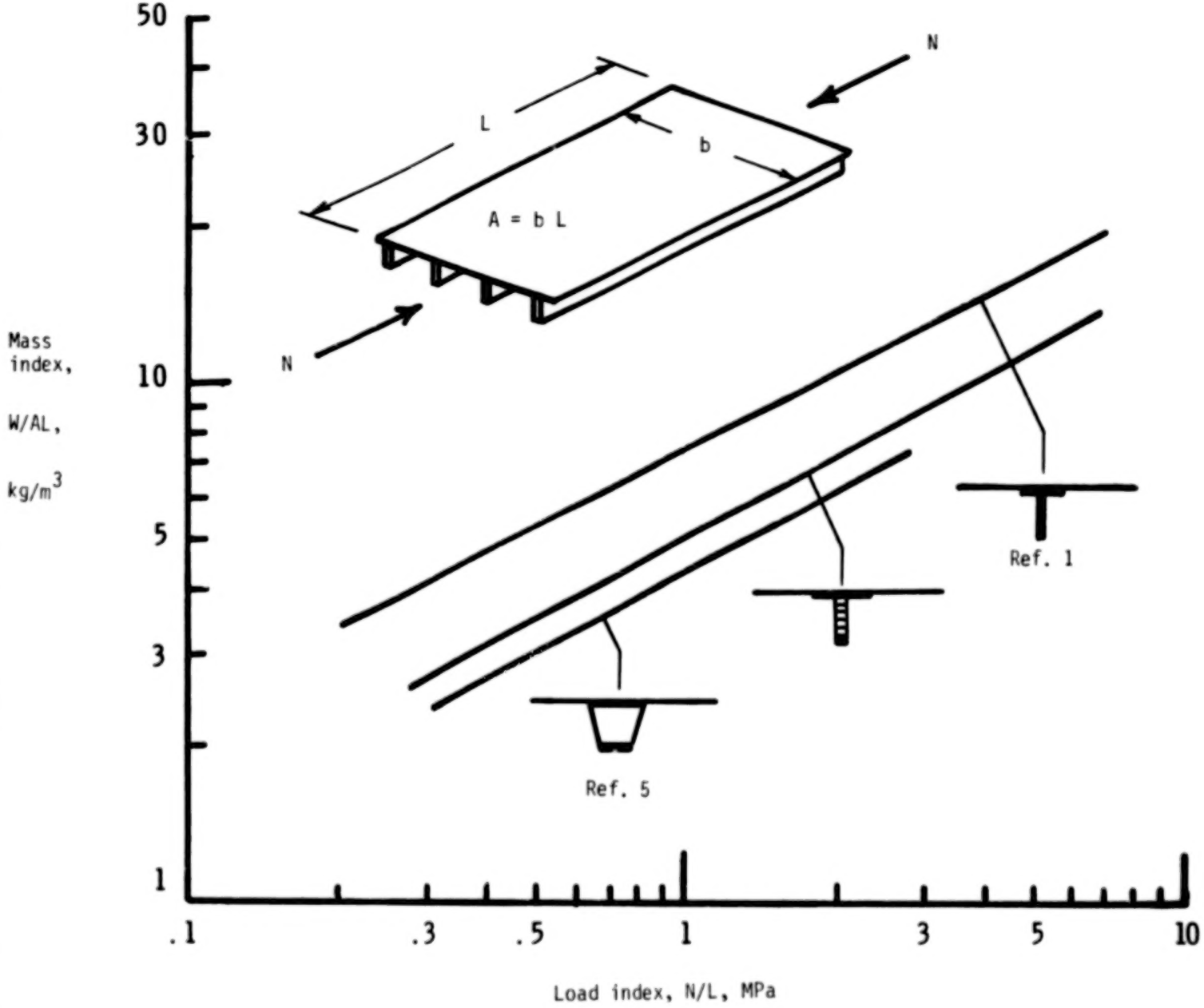

Figure 2.- Compression-load structural efficiency comparison for graphite/epoxy blade, sandwich-blade, and hat-stiffened panels. $kg/m^3 = 36.1 \times 10^{-6}$ lbm/in^3; MPa = 145 psi.

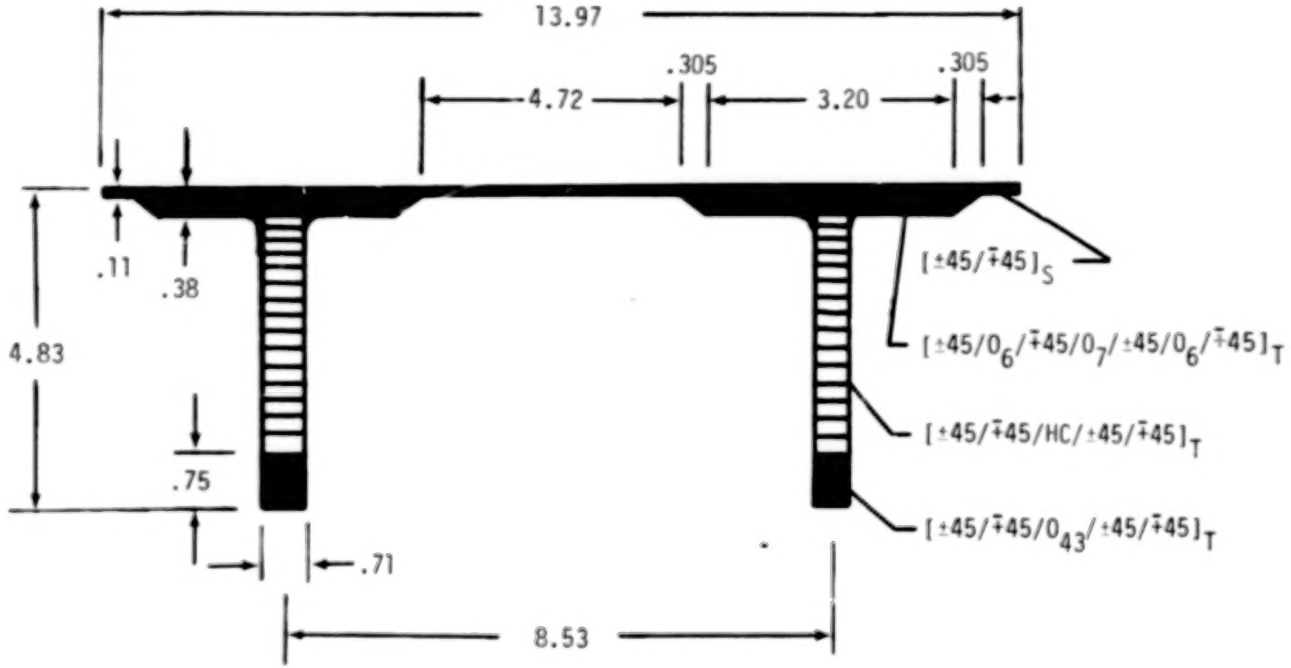

(a) Moderately loaded design.

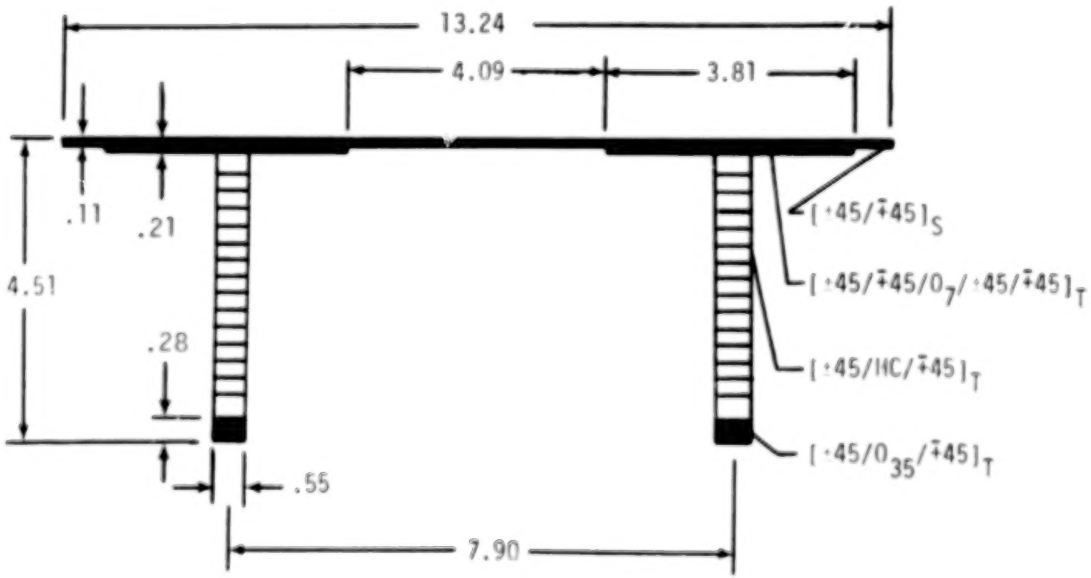

(b) Lightly loaded design.

Figure 3.- Cross-sectional dimensions of panel designs considered. (All dimensions are in centimeters.)

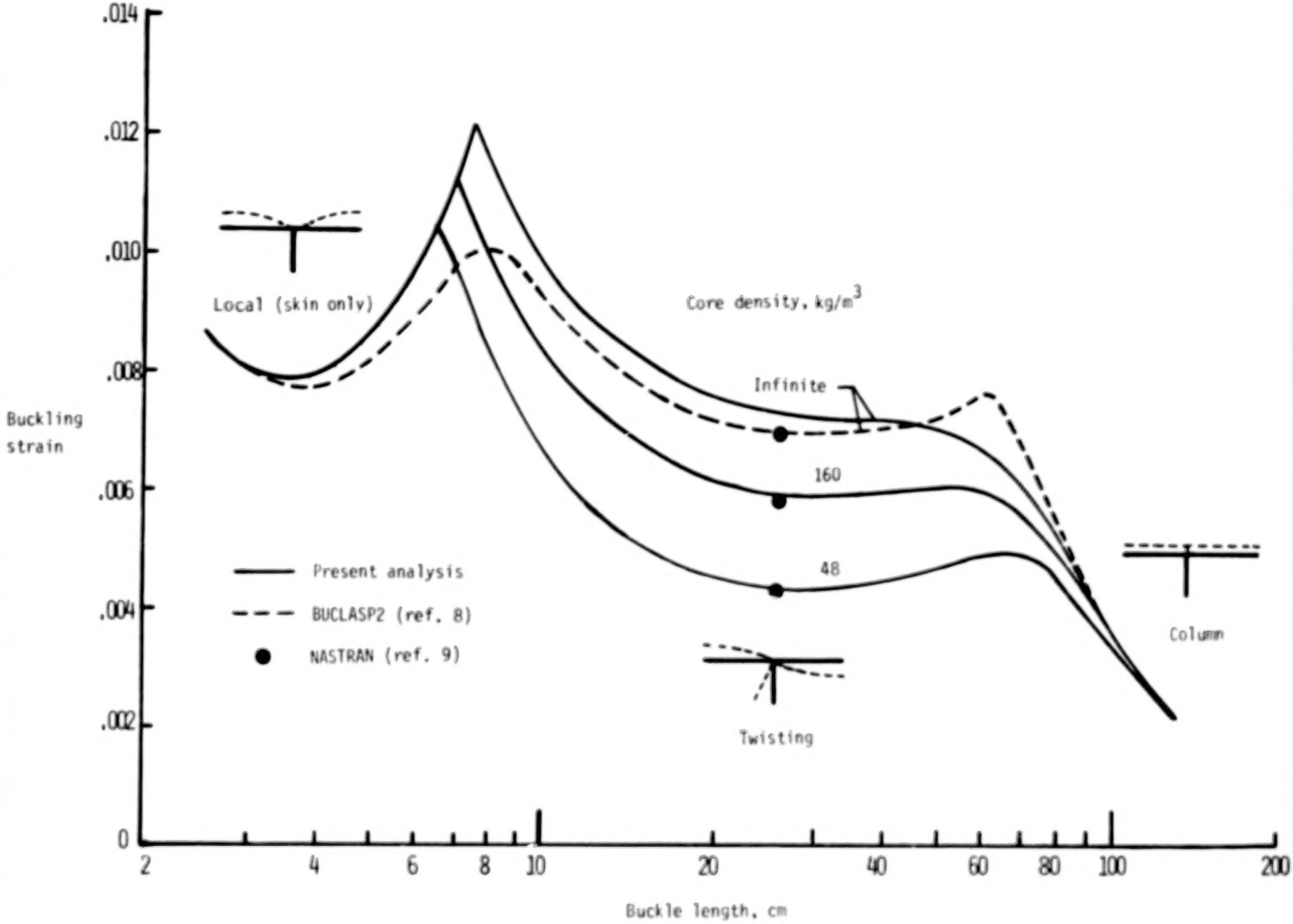

Figure 4.- Comparison of analytical results for compressive buckling strain of moderately loaded sandwich-blade stiffened composite panel with panel buckle length.

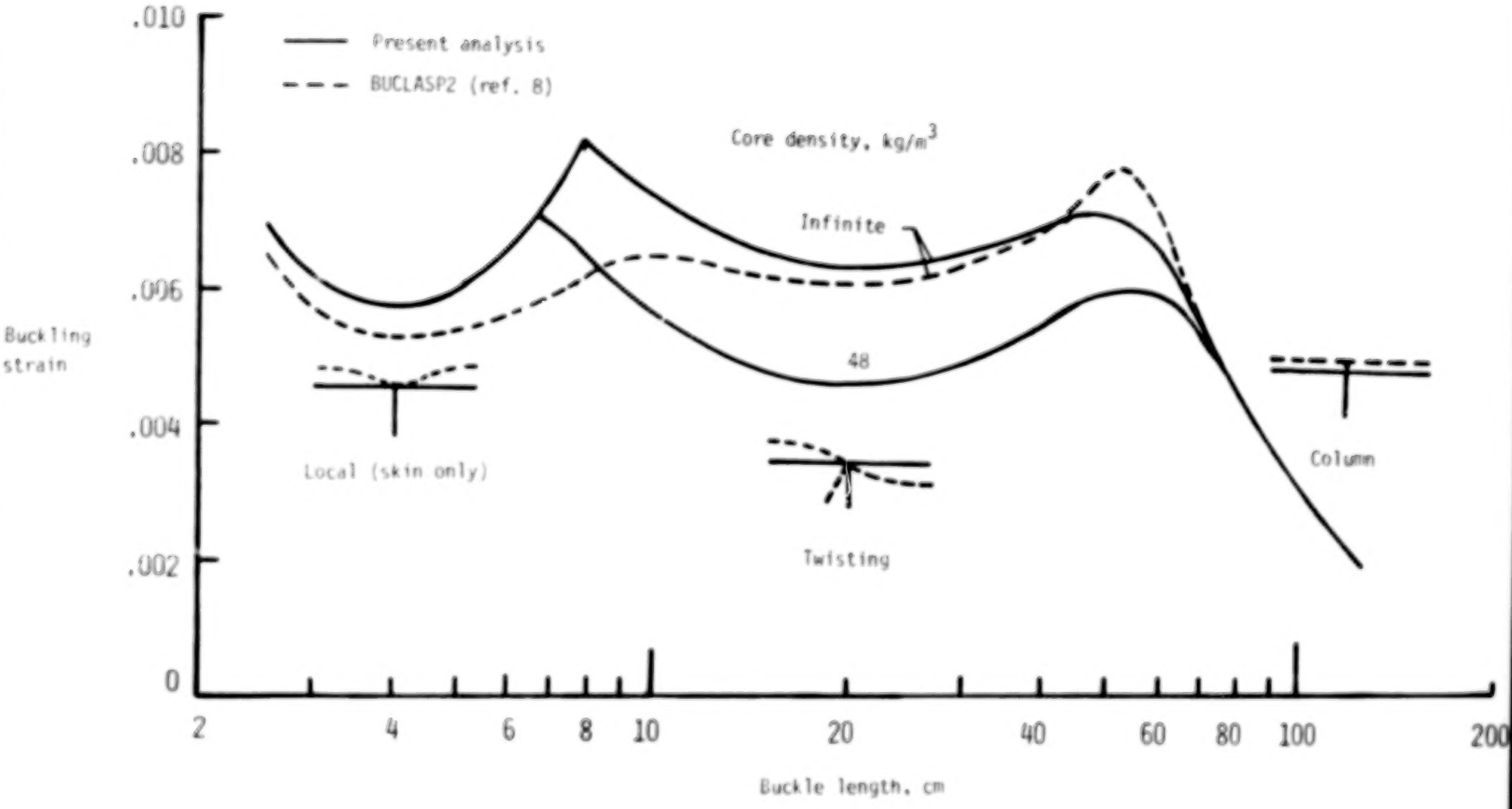

Figure 5.- Comparison of analytical results for compressive buckling strain of lightly loaded sandwich-blade stiffened composite panel with panel buckle length.

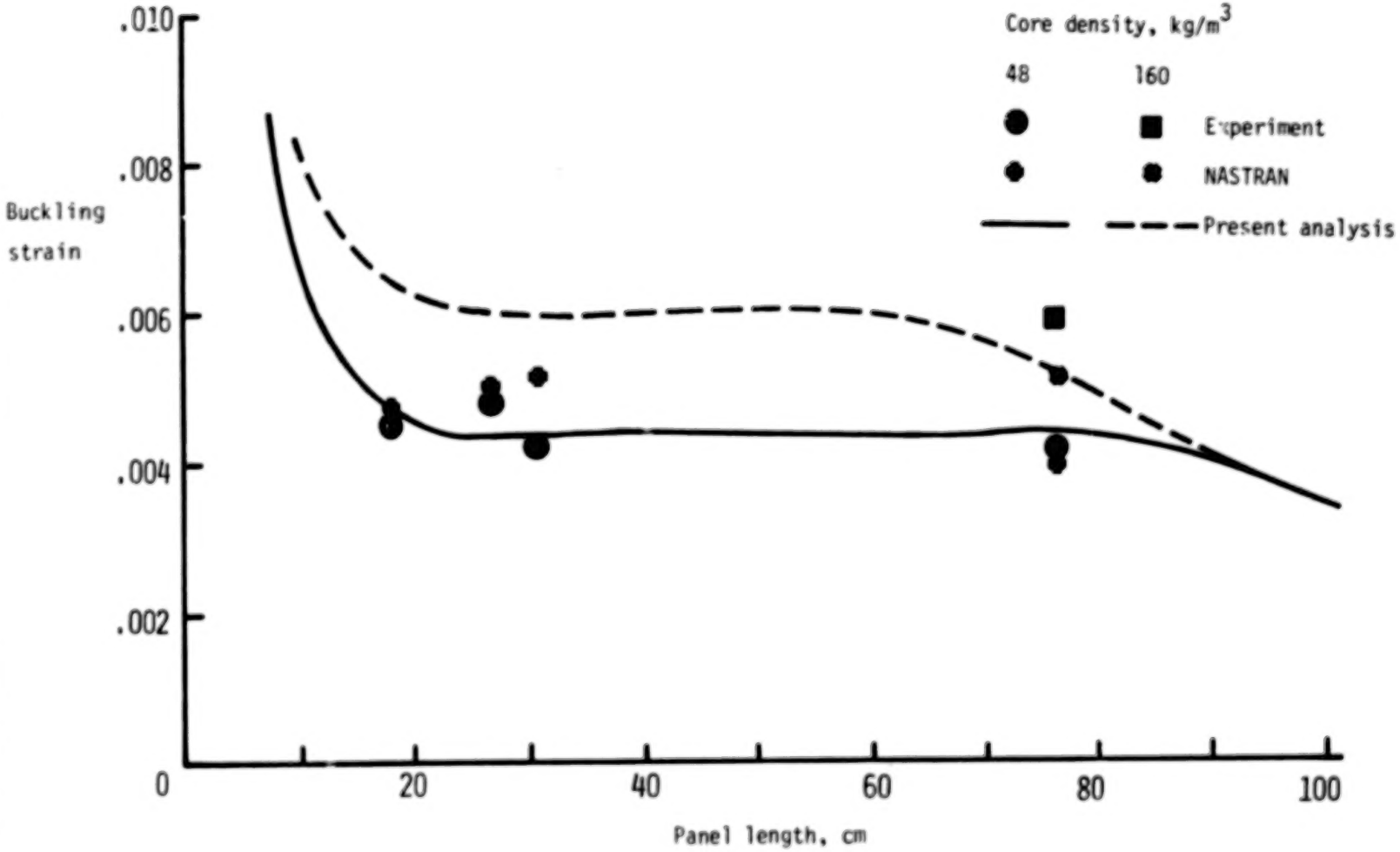

Figure 6.- Compressive buckling strains for moderately loaded sandwich-blade stiffened composite panel.

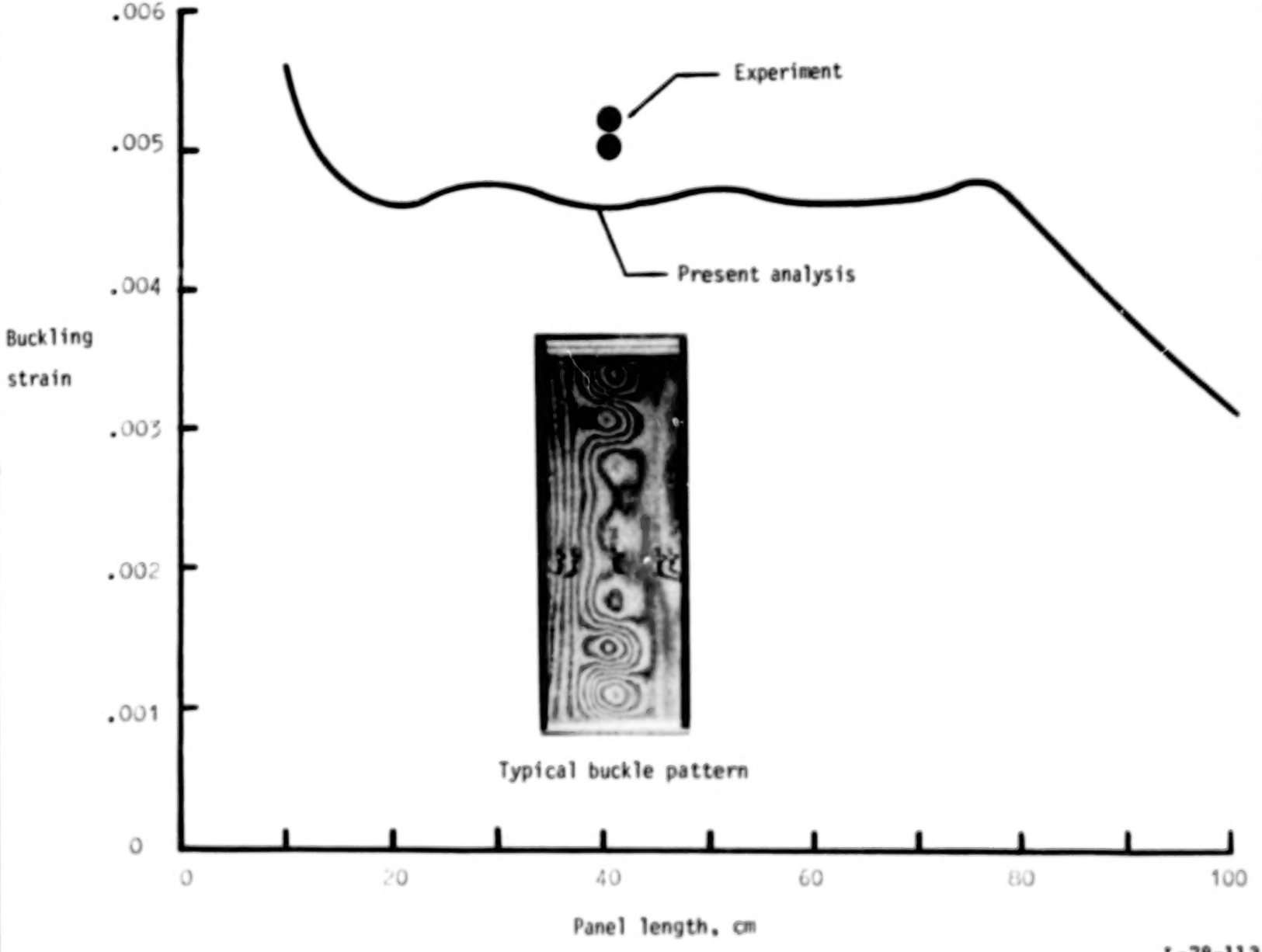

Figure 7.- Compressive buckling strains for lightly loaded sandwich-blade stiffened composite panel. Core density, 48 kg/m^3.

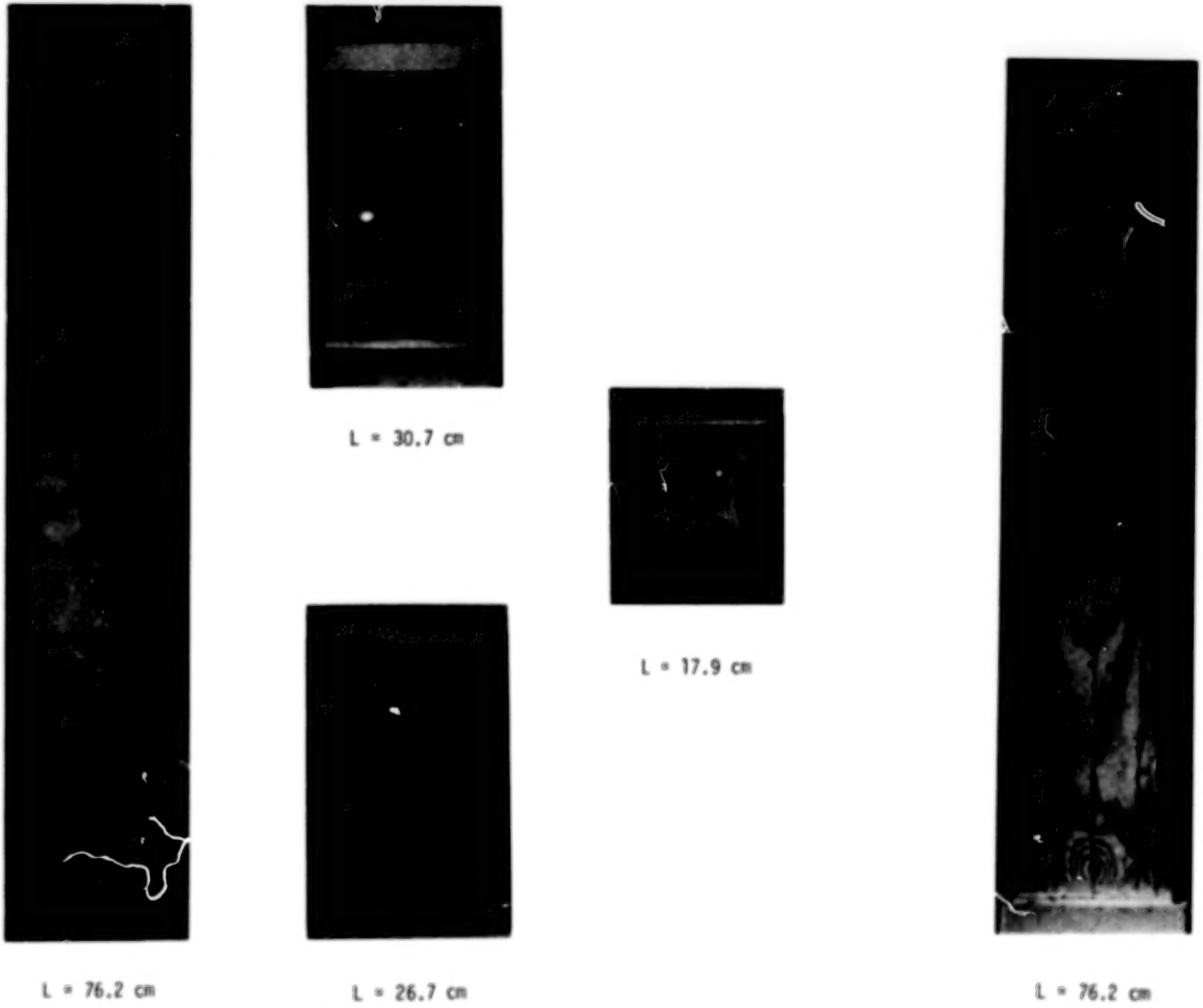

(a) 48 kg/m^3 aluminum-honeycomb core density.

(b) 160 kg/m^3 aluminum-honeycomb core density.

L-78-114

Figure 8.- Moire fringe patterns showing skin buckling of moderately loaded sandwich-blade stiffened composite panel.

1. Report No.	2. Government Accession No.	3. Recipient's Catalog No.
NASA TP-1269		

4. Title and Subtitle	5. Report Date
BUCKLING AND STRUCTURAL EFFICIENCY OF SANDWICH-BLADE STIFFENED COMPOSITE COMPRESSION PANELS	September 1978
	6. Performing Organization Code

7. Author(s)	8. Performing Organization Report No.
Manuel Stein and Jerry G. Williams	L-12242
	10. Work Unit No. 505-02-13-42

9. Performing Organization Name and Address	11. Contract or Grant No.
NASA Langley Research Center Hampton, VA 23665	

12. Sponsoring Agency Name and Address	13. Type of Report and Period Covered
National Aeronautics and Space Administration Washington, DC 20546	Technical Paper
	14. Sponsoring Agency Code

15. Supplementary Notes

16. Abstract

The minimum-mass structural efficiency curve is determined for sandwich-blade stiffened composite compression panels subjected to buckling and strength constraints. High structural efficiencies are attainable for this type of construction. A method of analysis is presented for the buckling of panels of this configuration which shows that buckling of such panels is strongly dependent on the through-the-thickness transverse shearing of the stiffener. Experimental results are presented and compared with theory.

17. Key Words (Suggested by Author(s))		18. Distribution Statement
Structural design	Minimum-mass design	Unclassified - Unlimited
Composite panels	Structural efficiency	
Compression panels	Buckling analysis	
Transverse shear	Sandwich constructions	
Stiffened panels	Structural synthesis	Subject Category 39

19. Security Classif. (of this report)	20. Security Classif. (of this page)	21. No. of Pages	22. Price*
Unclassified	Unclassified	37	$4.50

38

END

DEC 14 1978